

# SCIENTIFIC REPORTS

OPEN

## Bandgap reduction of photocatalytic TiO<sub>2</sub> nanotube by Cu doping

S. Khajoei Gharaei<sup>1</sup>, M. Abbasnejad<sup>1</sup> & Ryo Maezono<sup>2,3</sup>

We performed the electronic structure calculations of Cu-doped TiO<sub>2</sub> nanotubes by using density functional theory aided by the Hubbard correction (DFT + *U*). Relative positions of the sub-bands due to the dopants in the band diagram are examined to see if they are properly located within the redox interval. The doping is found to tune the material to be a possible candidate for the photocatalyst by making the bandgap accommodated within the visible and infrared range of the solar spectrum. Among several possibilities of the dopant positions, we found that only the case with the dopant located at the center of nanotube seems preventing from electron-hole recombinations to achieve desired photocatalytic activity with *n*-type behavior.

TiO<sub>2</sub> is a semiconductor with various polymorphs forming naturally or under high pressure and temperature, such as anatase, rutile and brookite or high pressure cotunnite and fluorite structures<sup>1–4</sup>, as representative phases. Its wider applications include sensors, photovoltaic and lithium batteries due to its exclusive photoelectronic properties, high chemical stability, low cost, and low environmental impacts<sup>5–9</sup>. It has a potential for controlling the environmental pollution, and for converting/storing energies. Its wide bandgap (3.2 eV) is, however, one of the matter hampering the improvements for more efficiency of devices working under the wide range of solar spectrum. So far, a lot of work has been done to investigate possible ways to reduce the bandgap<sup>10–14</sup>. Fabricating it in nanostructures is known to be one of the promising way by increasing the ratio of the surface to the volume. TiO<sub>2</sub> nanotubes (TiO<sub>2</sub>-NTs) have therefore attracted a lot of attentions in both experimental and theoretical researches investigating their unique optical and chemical properties due to high photocatalytic activity, strong oxidizing agents, and non-toxicity<sup>15</sup>.

However, it is reported that low-dimensional TiO<sub>2</sub> nanostructures tend to have the bandgap greater than 3.0 eV due to the quantum confinement effects<sup>16,17</sup>, getting rather toward less efficiency in the visible range of the solar spectrum. To make the bandgap back to be reduced less than 3.0 eV, the doping of impurities to the nanotubes is reported as a promising way<sup>18–20</sup>, which chemical stability is experimentally confirmed as well<sup>16</sup>. Cu doping has especially attracted its interest as a good candidate both experimentally and theoretically due to its high abundance with low cost availability<sup>21,22</sup>. In this work, we investigated such a possibility to get properly tuned bandgap by using *ab initio* electronic structure analysis.

To get a plausible model, both in the sense of computationally and geometrically, we constructed it carefully, step by step from a bulk to a pristine tube and to a Cu-doped tube: To justify our computational model (DFT + *U*), we carefully checked first whether the introduced *U* properly reproduced the available experimental values. After fixing the *U* parameter, we constructed a geometry model for the TiO<sub>2</sub>-NT by rolling up a possible surface cut from an anatase bulk. The bandgap evaluated for the pristine tube is confirmed to be consistent with those from other available reports<sup>15,23,24</sup>. Several possibilities of the Cu doping are examined over the cases with a dopant inserted inside the tube, attached on the surface of the tube, substituting titanium (Ti) site with and without an Oxygen (O) vacancy nearby. To the extent of the justification of our model (the limited system size, and the reliability within DFT), the case with a Cu dopant located at the center of nanotube is predicted to realize the reduced bandgap with the recombinations most unlikely to occur. The present result would support the ability of Cu-doped TiO<sub>2</sub>-NT as a candidate of photocatalytic materials, as reported experimentally by Momeni *et al.*<sup>25</sup>, showing that their nanotube improves the photocatalytic behavior.

<sup>1</sup>Faculty of Physics, Shahid Bahonar University of Kerman, Kerman, Iran. <sup>2</sup>School of Information Science, JAIST, Asahidai 1-1, Nomi, Ishikawa, 923-1292, Japan. <sup>3</sup>Computational Engineering Applications Unit, RIKEN, 2-1 Hirosawa, Wako, Saitama, 351-0198, Japan. Correspondence and requests for materials should be addressed to M.A. (email: [m\\_abbasnejad@uk.ac.ir](mailto:m_abbasnejad@uk.ac.ir))

| Method                       | $a$   | $c$   | $V_0$                               | $E_g$ | $B_0$ | $B'_0$ |
|------------------------------|-------|-------|-------------------------------------|-------|-------|--------|
|                              | (Å)   | (Å)   | (Å <sup>3</sup> /TiO <sub>2</sub> ) | (eV)  | (GPa) |        |
| GGA-PBE + $U$ [present work] | 3.893 | 9.663 | 36.61                               | 2.58  | 167   | 4.0    |
| GGA-PBE [present work]       | 3.796 | 9.579 | 34.51                               | 2.10  | 177   | 4.8    |
| GGA-PBE + $U$ <sup>11</sup>  | 3.834 | 9.632 | 35.40                               | 2.00  | —     | —      |
| GGA-PBE <sup>58</sup>        | 3.800 | 9.670 | 34.91                               | 2.25  | —     | —      |
| PBE <sup>59</sup>            | 3.786 | 9.867 | 35.36                               | —     | —     | —      |
| LDA <sup>60</sup>            | 3.758 | 9.495 | 33.52                               | —     | 194   | —      |
| Exp. <sup>20</sup>           | 3.784 | 9.507 | 34.03                               | 3.18  | —     | —      |
| Exp. <sup>61</sup>           | 3.785 | 9.511 | 34.07                               | —     | 179   | 4.5    |

**Table 1.** The calculated lattice parameters ( $a$  and  $c$ ), relaxed volume ( $V_0$ ), electronic band gap ( $E_g$ ), bulk modulus ( $B_0$ ) and its derivative ( $B'_0$ ) of anatase TiO<sub>2</sub> bulk structure compared to the other experimental and theoretical values.

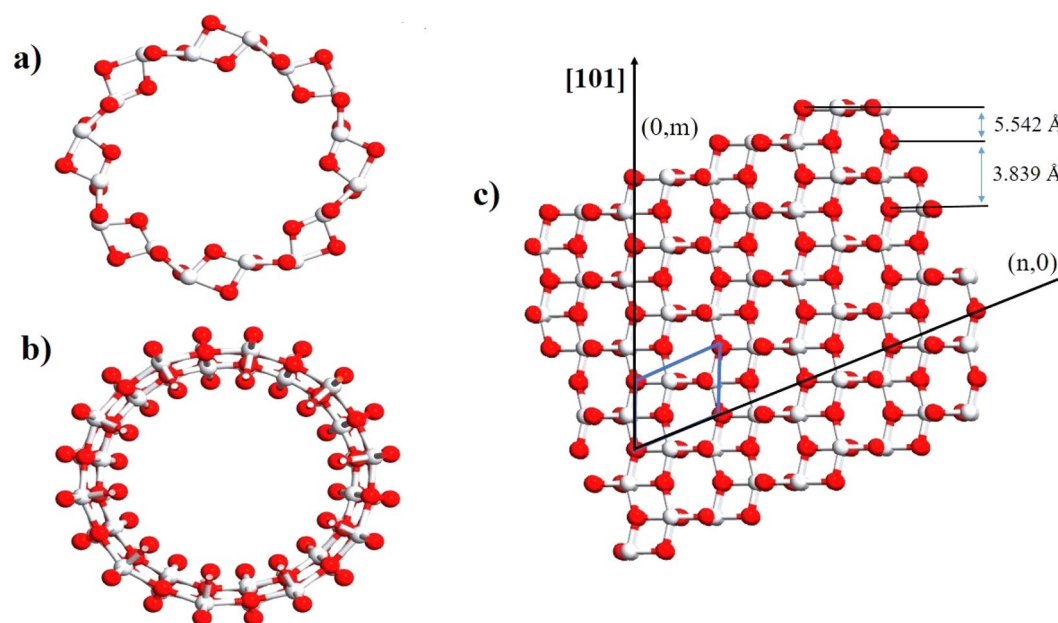


**Figure 1.** A general view of (a)  $(0, m)$ , (b)  $(n, 0)$  TiO<sub>2</sub>-NT, and (c)  $(101)$  surface of TiO<sub>2</sub>. The red and white spheres represent the O and Ti atoms, respectively.

## Results

All calculations were performed in the framework of DFT (density functional theory)<sup>26</sup> based on the plane wave and the pseudopotential method. Detailed descriptions for the method are given in the latter section. We used DFT +  $U$  scheme<sup>27</sup> since Ti in our system has half-filled  $d$  orbitals, for which the scheme is widely accepted as a reasonable choice. Since the choice of the Hubbard parameter ( $U$ ) strongly affects the reliability of predictions<sup>28</sup>, we have to calibrate it carefully taking some appropriate reference system. We took the anatase TiO<sub>2</sub> bulk for the reference because the phase has the highest photocatalytic activity among the other phases being appropriate for the purpose of the present study. Our choice,  $U = 4.2$  eV for Ti, gives a reasonable coincidence with experimental values, as summarized in Table 1.

Having fixed  $U$  for Ti, we performed the calculations for TiO<sub>2</sub>-NTs. The structure of the one-dimensional single-wall nanotube is formed by rolling up a possible surface of anatase TiO<sub>2</sub> bulk<sup>23</sup>. Though both  $(001)$  and  $(101)$  surfaces are known to be found in natural crystals, ultrathin  $(001)$  surfaces are reported being not feasible to form a tube due to its surface reconstructions<sup>15</sup>. We therefore took the  $(101)$  surface taken from the bulk (Table 1) to construct our nanotubes. Fig. 1 shows the geometry of the nanotube with different chiralities,  $(n, 0)$  and  $(0, m)$ . We considered only  $(0, m)$  because it is reported to realize less strain compared to  $(n, 0)$  under the same radius<sup>15,24</sup>. To make sure whether our nanotube structure could describe realistic samples to some extent, we examined the dependence of the calculated properties on  $m$ <sup>29</sup>, as tabulated in Table 2. All the computational details are given in Sec. ‘Computational Details’.

The evaluated dependence of the bandgap agrees with those by the other reported works in the sense that the semiconducting behavior is kept regardless of their chirality<sup>30</sup> while the increase of bandgap is observed as the tube diameter increases. From the dependence on  $m$ , we can estimate the bandgap to be compared with the

| nanotube | N  | D(Å)              |                   | T(Å)              |                   | $E_{form}$ (eV)   | $E_g$ (eV)        |                   |                   |
|----------|----|-------------------|-------------------|-------------------|-------------------|-------------------|-------------------|-------------------|-------------------|
|          |    | Before relaxation | After relaxation  | Before relaxation | After relaxation  |                   |                   |                   |                   |
| (0,3)    | 36 | 7.798             | 7.536             | 2.485             | 2.474             | 0.661             | 3.26              |                   |                   |
| (0,4)    | 48 | 10.683            | 10.368            | 2.488             | 2.478             | 0.626             | 3.46              |                   |                   |
| (0,5)    | 60 | 14.307            | 14.193            | 2.489             | 2.479             | 0.604             | 3.55              |                   |                   |
| (0,6)    | 72 | 17.488            | 17.395            | 2.490             | 2.480             | 0.589             | 3.61              |                   |                   |
|          |    | Ti-O (Å)          |                   |                   |                   |                   |                   |                   |                   |
|          |    | Before relaxation |                   |                   | After relaxation  |                   |                   |                   |                   |
| nanotube |    | Ti-O <sub>1</sub> | Ti-O <sub>2</sub> | Ti-O <sub>3</sub> | Ti-O <sub>4</sub> | Ti-O <sub>1</sub> | Ti-O <sub>2</sub> | Ti-O <sub>3</sub> | Ti-O <sub>4</sub> |
| (0,3)    |    | 1.958             | 2.000             | 1.708             | 1.961             | 1.988             | 1.864             | 1.836             | 2.070             |
| (0,4)    |    | 2.014             | 1.925             | 2.208             | 1.968             | 2.019             | 1.810             | 1.915             | 2.007             |
| (0,5)    |    | 1.967             | 2.168             | 1.933             | 2.013             | 2.012             | 1.931             | 1.800             | 2.010             |
| (0,6)    |    | 1.961             | 1.984             | 1.858             | 1.985             | 1.984             | 1.792             | 1.900             | 2.076             |

**Table 2.** The diameter ( $D$ ) and thickness ( $T$ ) of the pristine (0,  $m$ )-TiO<sub>2</sub>-NTs before and after relaxation.  $N$  is the number of atoms in the structure, and  $E_{form}$  and  $E_g$  are the formation energy and the electronic bandgap of the TiO<sub>2</sub>-NTs, respectively. For Ti-O bond lengths, each Ti atom is bonded to four O atoms as in Fig. 5 (left one). The O atoms are marked with numbers 1 to 4. For pristine NT, it is tractable upto  $m = 6$ , while when a Cu-dopant is attached,  $m = 3$  gets to be the tractable upper limit (see text).

experimental sample size. The estimation is fairly in consistent with the available experimental values, ranging 3.15–3.42 eV<sup>25,31–37</sup>. The dependence of the formation energy agrees with those reported in preceding works<sup>15,23,24</sup> as well, getting decreased as the diameter increases. The dependence of the bandgap on  $m$  might be related with the reported dependence of the photocatalytic activity on the system size<sup>38</sup>. A preceding theoretical analysis by a kinetic model<sup>38</sup> reports that the photocatalytic activity initially increases and then decreases as the diameter ( $D$ ) and the wall thickness ( $T$ ) increases, being attributed to the change in the light absorption, the surface area, and the reactant transport. Provided that the initial increase would be extrinsic due to some sample quality issues, the trend shown in Table 2 might properly be capturing the asymptotic decrease of the activity depending on  $T$  and  $D$ , regardless of the mismatch in the range of  $m$  between the experimental system size and our feasible range of it.

For modeling the Cu-doping, we considered four possibilities as shown in Fig. 2, the absorption of a Cu atom located at the center of the tube ('1/center-inserted'), at the surface of the tube ('2/surface-attached'), and the substitution by a Cu replacing a Ti site without ('3/substituted') and with an Oxygen vacancy ('4/substituted-with-vac'). We considered the substitution cases because the radius of Cu<sup>2+</sup> is near to that of Ti<sup>4+</sup>, being likely to replace the latter. For the O vacancy, it is reported to improve the optical absorption and the photocatalytic activity<sup>39,40</sup>. It is also reported that the addition of Cu impurities tends to create O vacancies for the charge compensation, making the optical absorption extending toward the visible-light range<sup>22</sup>. For the sake of tractability, we used  $m = 3$  for the system size to investigate the doping case. Calculations beyond  $m = 3$  are intractable at the present computational power even using a large commercial supercomputer, as described in Sec. 'Computational Details'. We ought to note that the present results, especially the predictions given in Fig. 3, are restrictive to the extent of the system size here. Photoexcitation phenomena include many-body effects which are known to be critically affected by the finite size errors<sup>41</sup>. The  $U$  parameter was also introduced for Cu being 5.2 eV taken from the other reports<sup>42</sup>. The value is reported to reproduce the features of experimental X-ray photoemission spectroscopies for Cu<sub>2</sub>O<sup>42</sup>. We considered the magnetic polarizations on Cu because more structural stability is found to be achieved by allowing the polarizations.

To get proper photocatalytic functions, it is known<sup>43</sup> for the candidate materials to satisfy the inequalities:

$$\varepsilon_{VB} < \varepsilon_{HOIL} < \varepsilon_{O_2/H_2O} < \varepsilon_{H^+/H_2} < \varepsilon_{LUIL} < \varepsilon_{CB} \quad (1)$$

where  $\varepsilon_{VB}$ ,  $\varepsilon_{CB}$ ,  $\varepsilon_{HOIL}$  and  $\varepsilon_{LUIL}$  denote the valance band top, the conduction band bottom, the highest occupied, and the lowest unoccupied impurity levels, respectively. A band-lineup diagram, as shown in Fig. 3, is used as a common way to distinguish the capabilities of materials for the photocatalytic functions. Taking the vacuum levels, given in Table 3, as the common reference level, four cases of Cu-doping are compared on the figure, with the oxidation and the reduction potential level of the water, marked  $\varepsilon_{O_2/H_2O}$  and  $\varepsilon_{H^+/H_2}$ , respectively.

We can see that newly created impurity levels appear inside the gap, leading to the reduction of the bandgap as tabulated in Table 4. These reduced bandgaps are accommodated within the energy range of the solar light (1.5–2.8 eV), except '3/substituted'. By the partial DOS analysis given in Sec. 'Computational Details', we can identify the impurity levels mainly coming from Cu-3*d* and -4*s*. More multiplicity of the levels seen for '2/surface-attached' and '3/substituted' cases is because of the hybridization with O-2*p* state nearby the Cu site. For the 'center-inserted' case, the conduction band gets lower to touch the Fermi level, giving *n*-type behavior.

From Fig. 3, we can immediately found that '1/center-inserted' is the best candidate while in other cases impurity levels are located within the redox interval, [ $\varepsilon_{O_2/H_2O}$ ,  $\varepsilon_{H^+/H_2}$ ], implying the possibility of the recombinations of excitations. Having such a candidate would support the capability of Cu-doped TiO<sub>2</sub> nanotubes as a photocatalytic material<sup>25</sup> to some extent, though the present prediction should be restricted within the limitation of the present computational model (tractable system size, and DFT-limited treatments of many-body effects for excitations).

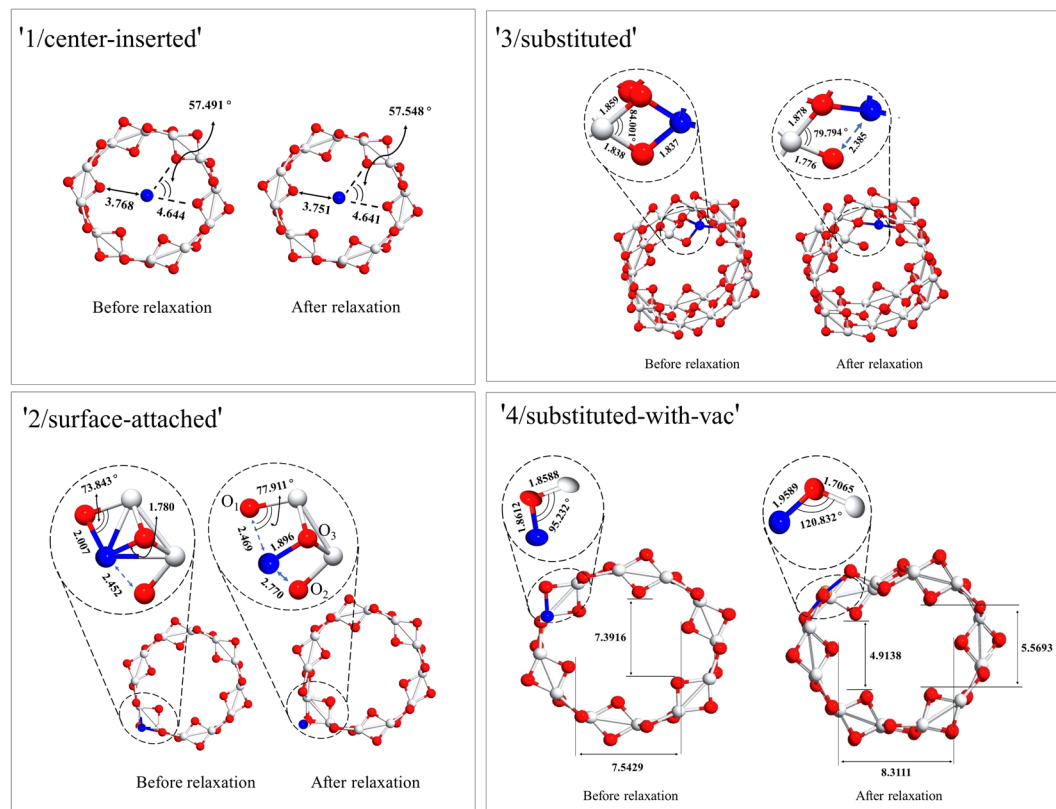


**Figure 2.** Four cases considered for the Cu-doping model. White, red and blue spheres represent Ti, O and Cu atoms, respectively. All distances are in unit of Angstrom.

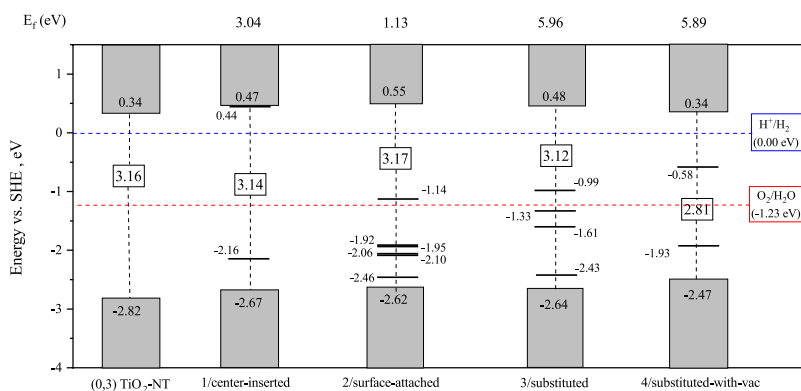


**Figure 3.** Band-structure diagram for pure and Cu-doped  $\text{TiO}_2$ -NTs in different configurations. The blue and red dotted line are the redox potentials,  $\varepsilon_{\text{H}^+/\text{H}_2}$  and  $\varepsilon_{\text{O}_2/\text{H}_2\text{O}}$ , respectively. The zero of the energy scale corresponds to the potential of the standard hydrogen electrode SHE ( $\varepsilon_{\text{H}^+/\text{H}_2}$ ), which explains the difference to the one-electron levels in respect to vacuum zero as presented in Table 3. Solid horizontal lines describe  $\varepsilon_{\text{HOIL}}$  and  $\varepsilon_{\text{LUIL}}$  levels, below and above the redox potential  $\varepsilon_{\text{H}^+/\text{H}_2}$ , respectively. The rectangles correspond to the difference between the conduction and the valence bands.  $E_f$  values shown at the top are the formation energies of the proposed structures.

While the ‘1/center-inserted’ case is shown to be the most promising for the desired reaction, the geometry is likely to be unstable from its energetics. The formation energies of the four cases,  $E_f^{(1-4)}$ , are evaluated as given in Sec. ‘Computational Details’, shown in Fig. 4 as the dependence on the chemical potential of O ( $\mu_{\text{O}}$ ). The values under the O-rich condition are also shown in Fig. 3. Compared with ‘2/surface-attached’ case, ‘1/center-inserted’ requires higher energy (+3.04 eV) to form the doped Cu located at the center. Though the higher formation energy would be required to form the geometry, we might expect the local stability for a Cu to be kept at the center against tiny displacement. We examined such possibility by looking at the energy variation when a Cu is

| Structure                          | Fermi Level | Vacuum Level | Work Function |
|------------------------------------|-------------|--------------|---------------|
| Pristine (0,3) TiO <sub>2</sub> NT | -4.275      | 1.698        | 5.973         |
| 1/center-inserted                  | -2.144      | 1.734        | 3.878         |
| 2/surface-attached                 | -2.892      | 1.711        | 4.603         |
| 3/substituted                      | -4.519      | 1.682        | 6.201         |
| 4/substituted-with-vac             | -4.559      | 1.688        | 6.247         |

**Table 3.** Energetics required for the band-lineup diagram (Fig. 3). Units are all given in [eV].

| Structure                           | Highest occupied band |           | Lowest unoccupied band |           | $E_g$   |           |
|-------------------------------------|-----------------------|-----------|------------------------|-----------|---------|-----------|
|                                     | Spin-up               | Spin-down | Spin-up                | Spin-down | Spin-up | Spin-down |
| Pristine (0,3) TiO <sub>2</sub> -NT | -2.82                 |           | 0.34                   |           | 3.16    |           |
| 1/center-inserted                   | -2.16                 |           | 0.44                   |           | 2.60    |           |
| 2/surface-attached                  | -1.92                 | -1.14     | 0.55                   | 0.55      | 2.47    | 1.69      |
| 3/substituted                       | -2.64                 | -2.43     | -1.33                  | -1.61     | 1.31    | 0.82      |
| 4/substituted-with-vac              | -1.93                 | -2.47     | 0.34                   | -0.58     | 2.27    | 1.89      |
| Bulk TiO <sub>2</sub>               | 0.05                  |           | 2.63                   |           | 2.58    |           |

**Table 4.** The values of the highest occupied and the lowest unoccupied band as well as the electronic bandgap of the TiO<sub>2</sub>-NT structures. Units are all given in [eV].

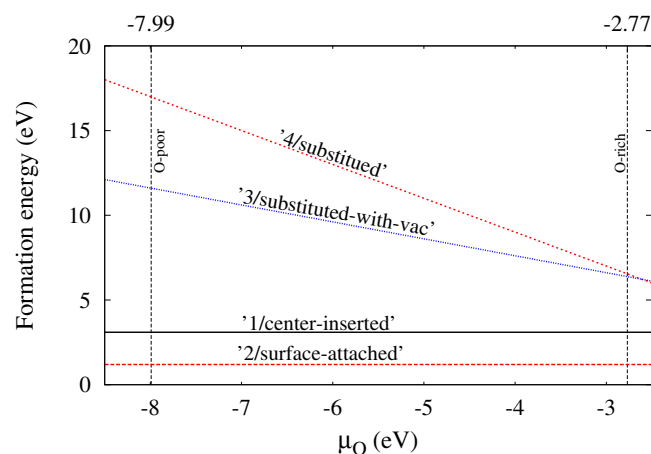


**Figure 4.** Calculated Formation energy of four cases considered for the Cu-doping model versus chemical potential of O ( $\mu_{\text{O}}$ ) in the allowed interval.

displaced from the center, but the result could not support such possibility, giving the energy *increasing* corresponding to the local *maximum* energetically. It might be possible to attribute the observed transient property (photocatalyst activities decay in  $\sim 100$  [sec.])<sup>25</sup> to this instability of a Cu at nanotube center. Furthermore, it would be likely to attribute their observed enhancement of photocatalytic activity to that realized by '1/center-inserted' because a relevant experimental work<sup>44</sup> did not found CuO peak in their XRD, implying that the doped Cu would be located not on the surface<sup>44</sup>.

## Conclusion

Structural and electronic properties of the anatase TiO<sub>2</sub>-NT were investigated for the pristine and the Cu-doped cases within GGA-PBE +  $U$  framework. The present computational modeling, especially the choice of the Hubbard  $U$  parameters for Ti and Cu, and the geometrical construction of the nanotube is confirmed to give fairly good agreements with available experimental data. To the extent of the tractable system size, the reported trend of the properties on the nanotube diameter is fairly well reproduced. We examined four possible models of the Cu-doped nanotube to investigate the capability for the photocatalytic activity, over the geometries with a Cu inserted to the center of tube, attached on the tube surface, and substitution of Ti site with and without an Oxygen vacancy. For all these cases, the introduced Cu gives impurity levels appearing in between the bandgap of the pristine case, leading effective reductions of the bandgap. Except the case with a Cu inserted to the center of the tube, the impurity levels are located within the redox interval, corresponding to the possibility of the recombinations of excitations. The case with the 'center-inserted Cu' satisfies the condition with  $n$ -type behavior that the conduction



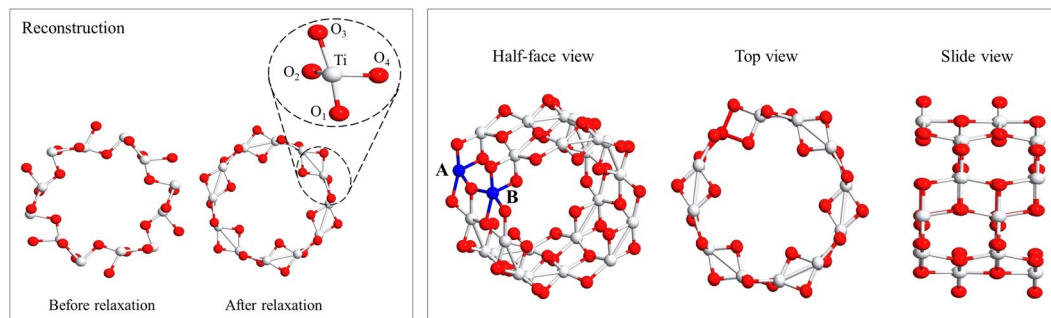


**Figure 5.** The geometrical reconstruction of (0,3)  $\text{TiO}_2$ -NT from the bulk structure (left panel) and the  $1 \times 1 \times 2$   $\text{TiO}_2$ -NT unit cell from different view (right panel). The red and white spheres represent the O and Ti atoms, respectively. Ti atom of type A and B are in blue color.

band and valance band edges located outside of the redox interval without such a possibility of recombinations, supporting the capability of such Cu-doped  $\text{TiO}_2$  nanotubes as a photocatalytic material<sup>25</sup>.

### Computational Details

For PW (plane wave)-DFT calculations, we used quantum ESPRESSO package<sup>45</sup>, with ultrasoft pseudopotentials<sup>46</sup>. The valence electronic states of Ti and O were considered as 3s, 3p, 4s, 3d and 2s, 2p, respectively. The pseudopotential of the Cu dopant was considered with the valence state, 3d and 4s. For the DFT +  $U$ <sup>27</sup> scheme, we used GGA-PBE exchange-correlation functional<sup>47</sup>. The Hubbard parameter ( $U$ ) for Ti is determined so that the calculated fundamental quantities (bandgap, bulk modulus *etc.*) can achieve reasonable coincidences to experimental values of the anatase  $\text{TiO}_2$  bulk. Convergence tests are performed to determine our final choice,  $E_{\text{cut}} = 40$  Ry (cutoff energy for plane wave expansions) and  $4 \times 4 \times 4$   $k$ -point grid. Cell and atomic positions are relaxed until the forces on each atom get to the less than 1.05 meV/Å, which is feasible to be applied to all the following nanotube cases with a common condition. We adapted  $U = 4.2$  eV for Ti taken from other works, which corrects the bandgap closer to the experimental value as shown in Table 1. Though the coincidence would be not so excellent within our GGA-PBE +  $U$ , we kept  $U$  untouched because it was adjustably obtained to give the correct splitting between occupied and unoccupied Ti- $d$  states for O vacancies at the rutile  $\text{TiO}_2$  (110) surface<sup>48</sup>, and has been used to model both native  $n$ -type defects, and the (Nb,Ta)-doping in the anatase  $\text{TiO}_2$ <sup>49,50</sup>. Moreover, the choice of  $U$  greater than 4 eV is reported to handle the electronic defects well<sup>51</sup>.

For (0,  $m$ ) nanotubes, we took the same  $E_{\text{cut}}$  as that for the bulk because the same pseudopotentials are applied. To capture the property of an isolated tube by the plane wave framework, the tube is located inside a periodic box with an enough large spacing between parallel tubes by 30 Å, being confirmed to reduce spurious interactions between neighboring tubes within  $10^{-6}$  eV. To make it tractable even when a Cu dopant is introduced, we took its unitcell as the multiple,  $1 \times 1 \times 2$ , of the original unitcell for a bulk, namely twice larger supercell along the tube extending direction, which contains 72 atoms, as shown in Fig. 5. The Brillouin zone along the extending direction is discretized into four grid points to get the band dispersion. To make meaningful comparisons of the bandgap between bulk and tube cases, we carefully checked to choose the computational conditions so that they can be common to the both cases achieving the convergence with respect to the parameters.

It is observed that the geometrical reconstruction from the bulk structure makes it more symmetric with the reductions in the diameter and the thickness, as shown in Fig. 5 for instance with (0,3)-NT case. Corresponding numerical results are tabulated in the Table 2. It is found that the reduction of the diameter during the reconstruction is attributed to the reductions of the Ti-O bond lengths along the normal direction to the tube surface. This may be due to the change of the coordination number of O between bulk and nanotube due to the change of curvature<sup>23</sup>.

The electronic band dispersion along the tube extending direction for (0,3)-nanotube as well as its total density of states (DOS) is given in Fig. 6. The indirect bandgap, 3.26 eV, is estimated being enhanced from that of bulk structure, 2.58 eV as given in Table 1. We note that the size of  $m = 3$  is far smaller than the size of the practical  $\text{TiO}_2$ -NTs, which outer diameters ranging 8–10 nm with an internal diameter being  $\sim 5$  nm<sup>52</sup>. When a Cu dopant is attached, however, the size of the computational model beyond  $m = 3$  gets to be too large to be handled even using a large commercial supercomputer (*e.g.*, Cray-XC40 we used here). This is not only because of the larger number of particles to be calculated (requiring more memory capacity), but also due to the exploding number of the freedom during the structural optimizations (even for  $m = 3$ , it took approximately one month for each case).

The formation energy of the nanotube tabulated in Table 2 is defined and evaluated as,

$$E_{\text{form}} = \frac{1}{n}(E_{\text{total}} - nE_{\text{bulk}}), \quad (2)$$

as a normalized difference between the total energy of the system,  $E_{\text{total}}$ , and that of the pristine bulk,  $E_{\text{bulk}}$  (per a  $\text{TiO}_2$  unit), where  $n$  is the number of the units included in the system.

For Cu-doped model, we considered four cases, ‘1/center-inserted’, ‘2/surface-attached’, and ‘3,4/substituted (with-vac)’, as explained in Sec. ‘Result’. Figure 7 shows the electronic band structure, total and partial density

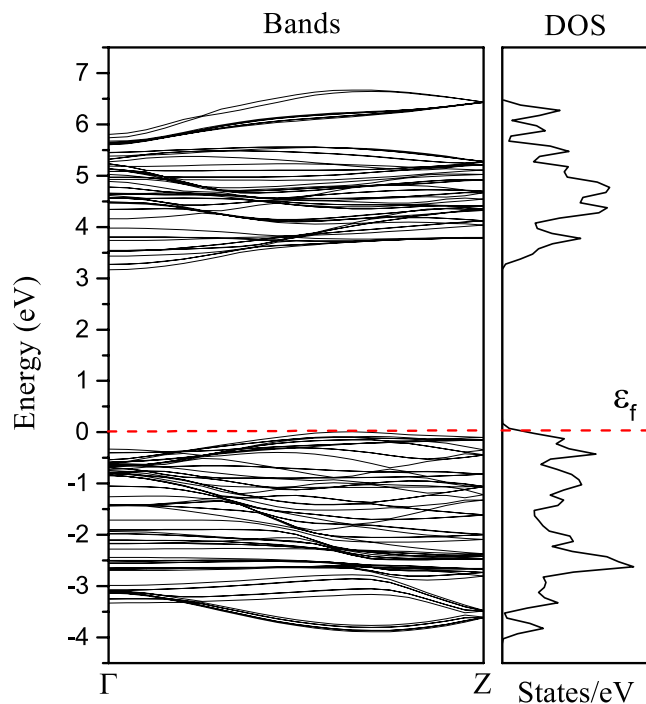


**Figure 6.** Electronic band dispersion along the tube extending direction and total DOS of pristine (0,3) TiO<sub>2</sub>-NT.

of states (DOS) for ‘1/center-inserted’ and ‘2/surface-attached’ cases. For each case, we can see newly appearing sub-bands due to the introduced Cu, as discussed in Sec. ‘Results’. For both cases, we performed spin polarized calculations getting significant magnetizations,  $0.58 \mu_B/\text{cell}$  on Cu (for ‘1/center-inserted’) and  $-1.00 \mu_B/\text{cell}$  on Ti (for ‘2/surface-attached’).

For the substitution case, there are two possibilities for a Ti site to be replaced by a Cu, marked as A and B in Fig. 5. Though they are different in their number of Ti-O bonds (four or five, respectively), we confirmed that the same structure is obtained after the relaxation regardless of each initial substitution. The schematic pictures showing geometrical change during the relaxation are given in Fig. 2, showing a slight compression of tube from top to bottom. The electronic band structure, total and partial DOS for the ‘3,4/substituted (with-vac)’ are also shown in Fig. 7. Similar to the ‘attached/inserted’ cases, we found several sub-bands appearing due to the introduced Cu and its hybridization with the neighboring Oxygen atoms when possible, as supported by the partial DOS identifying main ingredients. Spin polarized calculations conclude that the pronounced magnetizations appear on two O atoms neighboring to a Cu by  $0.36 \mu_B/\text{cell}$  and  $0.67 \mu_B/\text{cell}$ , respectively for ‘3/substituted’ case, while for ‘4/substituted-with-vac’,  $0.49 \mu_B/\text{cell}$  on Cu and  $0.17 \mu_B/\text{cell}$  on O, respectively.

To compose the band-lineup diagram (Fig. 3), we evaluated the work functions, shown in Table 3, using a scheme given in the literature<sup>53</sup>. We ought to note that the calculated work functions are overestimated when compared with experimental values ( $\sim 4.90 \text{ eV}$ <sup>54</sup>) by 20%. Similar overestimations are also reported for the cases of carbon nanotube models when being smaller than 10 Å in diameters<sup>55</sup>, being attributed to the downshift of Fermi levels due to the curvature effect.

To discuss the stability of the doped structures, we also evaluated the formation energy to introduce a Cu dopant into a pristine TiO<sub>2</sub>-NT. To distinguish with  $E_{\text{form}}$  (formation energy to construct a NT), we shall use a different notation with the definition<sup>56</sup>,

$$\begin{aligned} E_f^{(1,2)} &= E_{\text{tot}}(\text{Cu: Ti}_{24}\text{O}_{48}) - E_{\text{tot}}(\text{Ti}_{24}\text{O}_{48}) - \mu_{\text{Cu}}, \\ E_f^{(3)} &= E_{\text{tot}}(\text{Cu: Ti}_{23}\text{O}_{48}) - E_{\text{tot}}(\text{Ti}_{24}\text{O}_{48}) - \mu_{\text{Cu}} + \mu_{\text{Ti}}, \\ E_f^{(4)} &= E_{\text{tot}}(\text{Cu: Ti}_{23}\text{O}_{47}) - E_{\text{tot}}(\text{Ti}_{24}\text{O}_{48}) - \mu_{\text{Cu}} + \mu_{\text{Ti}} + \mu_{\text{O}}, \end{aligned} \quad (3)$$

where the upper suffix ( $i=1-4$ ) corresponds to four geometries such as ‘1/center-inserted’. Chemical potentials,  $\mu_{\text{Ti,Cu,O}}$ , are basically determined by the experimental growth conditions.  $\mu_{\text{Cu}}$  was considered as the energy of a Cu atom in the bulk structure.  $E_f^{(1,2)}$  is evaluated being  $+3.04 \text{ eV}$  ( $+1.13 \text{ eV}$ ) for the ‘1/center-inserted’ (‘2/surface-attached’) case, as shown in Fig. 3. For the cases of ‘3,4/substituted (with-vac)’, the chemical potentials are determined so that they can satisfy the following criterion under thermodynamic equilibrium,

$$\Delta H_f(\text{TiO}_2) = \mu_{\text{Ti}} + 2\mu_{\text{O}}, \quad (4)$$

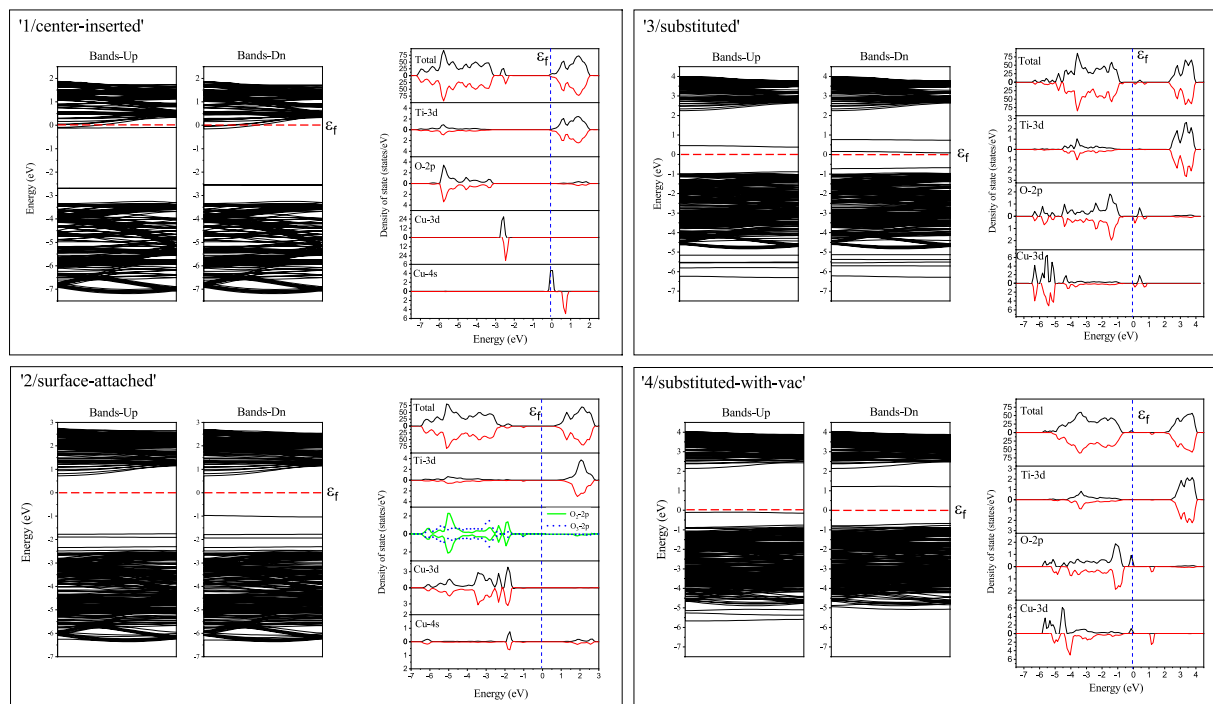


**Figure 7.** The electronic band structure along with the total and partial DOS of four cases considered for the Cu-doping model.

where  $\Delta H_f(\text{TiO}_2)$  is the enthalpy of the formation of the bulk  $\text{TiO}_2$ . The upper bounds of  $\mu_{\text{O}}$  and  $\mu_{\text{Ti}}$  can be obtained from the total energies of O molecule ( $E_{\text{tot}}(\text{O}_2)$ ) and the Ti atom in its bulk structure ( $E_{\text{tot}}(\text{Ti}_{\text{hcp}})$ ), respectively. The allowed range of  $\mu_{\text{O}}$  is therefore given as,

$$\frac{1}{2}(\Delta H_f(\text{TiO}_2) + E_{\text{tot}}(\text{O}_2)) \leq \mu_{\text{O}} \leq \frac{1}{2}E_{\text{tot}}(\text{O}_2), \quad (5)$$

corresponding to ‘O-poor’ and ‘O-rich’ conditions in the experimental growth processes. Our  $\Delta H_f(\text{TiO}_2)$  is evaluated as  $-10.20$  eV being in close agreement with the experimental value ( $-9.80$  eV)<sup>57</sup>, measured at the growth condition. Corresponding to the variation of  $\mu_{\text{O}}$ ,  $E_f$  for ‘3,4/substituted (with-vac)’ varies via relation, Eq. (4), as shown in Fig. 4. Formation energies for ‘3/substituted’ and ‘4/substituted-with-vac’ are evaluated to get 5.96 eV and 5.89 eV under the O-rich condition, respectively, showing little stabilization without the vacancy.

## Data Availability

All data generated or analysed during this study are included in this published article.

## References

- Shojaee, E. & Mohammadzadeh, M. First-principles elastic and thermal properties of  $\text{TiO}_2$ : a phonon approach. *J. Physics: Condens. Matter* **22**, 015401 (2009).
- Shojaee, E., Abbasnejad, M., Saedian, M. & Mohammadzadeh, M. First-principles study of lattice dynamics of  $\text{TiO}_2$  in brookite and cotunnite structures. *Phys. Rev. B* **83**, 174302 (2011).
- Abbasnejad, M., Shojaaee, E., Mohammadzadeh, M., Alaei, M. & Maezono, R. Quantum Monte Carlo study of high-pressure cubic  $\text{TiO}_2$ . *Appl. Phys. Lett.* **100**, 261902 (2012).
- Abbasnejad, M., Mohammadzadeh, M. & Maezono, R. Structural, electronic, and dynamical properties of pca21- $\text{TiO}_2$  by first principles. *EPL Europhysics Lett.* **97**, 56003 (2012).
- Li, X., Xiong, R. & Wei, G. Preparation and photocatalytic activity of nanoglued Sn-doped  $\text{TiO}_2$ . *J. Hazard. Mater.* **164**, 587–591 (2009).
- Ardizzone, S. *et al.* Tailored anatase/brookite nanocrystalline  $\text{TiO}_2$ . The optimal particle features for liquid- and gas-phase photocatalytic reactions. *The J. Phys. Chem. C* **111**, 13222–13231 (2007).
- Li, M., Tang, P., Hong, Z. & Wang, M. High efficient surface-complex-assisted photodegradation of phenolic compounds in single anatase titania under visible-light. *Colloids Surfaces A: Physicochem. Eng. Aspects* **318**, 285–290 (2008).
- Li, M., Hong, Z., Fang, Y. & Huang, F. Synergistic effect of two surface complexes in enhancing visible-light photocatalytic activity of titanium dioxide. *Mater. Res. Bull.* **43**, 2179–2186 (2008).
- Trail, J., Monserrat, B., Rios, P. L., Maezono, R. & Needs, R. J. Quantum Monte Carlo study of the energetics of the rutile, anatase, brookite, and columbite  $\text{TiO}_2$  polymorphs. *Phys. Rev. B* **95**, 121108 (2017).
- Finazzi, E., Di Valentin, C., Selloni, A. & Pacchioni, G. First principles study of nitrogen doping at the anatase  $\text{TiO}_2$  (101) surface. *The J. Phys. Chem. C* **111**, 9275–9282 (2007).
- Araujo-Lopez, E., Varilla, L. A., Seriani, N. & Montoya, J. A.  $\text{TiO}_2$  anatase’s bulk and (001) surface, structural and electronic properties: A DFT study on the importance of hubbard and van der waals contributions. *Surf. Sci.* **653**, 187–196 (2016).
- Li, C., Dang, S., Zhang, C., Wang, L. & Han, P. Effects of native defects on the electronic structure and photocatalytic activity in anatase  $\text{TiO}_2$  by first principles calculations. *Optik-International J. for Light. Electron Opt.* **125**, 3145–3149 (2014).



13. Sotoudeh, M., Abbasnejad, M. & Mohammadizadeh, M. R. First principles study of hydrogen doping in anatase TiO<sub>2</sub>. *The Eur. Phys. Journal-Applied Phys.* **67** (2014).
14. Sotoudeh, M., Hashemifar, S., Abbasnejad, M. & Mohammadizadeh, M. *Ab-initio* study of hydrogen doping and oxygen vacancy at anatase TiO<sub>2</sub> surface. *AIP Adv.* **4**, 027129 (2014).
15. Hai-Yang, Z. & Shun-Le, D. First principles study of single wall TiO<sub>2</sub> nanotubes rolled by anatase monolayers. *Chin. Phys. Lett.* **30**, 043102 (2013).
16. Mowbray, D., Martinez, J. I., García Lastra, J., Thygesen, K. S. & Jacobsen, K. W. Stability and electronic properties of TiO<sub>2</sub> nanostructures with and without B and N doping. *The J. Phys. Chem. C* **113**, 12301–12308 (2009).
17. Cherian, R., Gerard, C., Mahadevan, P., Cuong, N. T. & Maezono, R. Size dependence of the bulk modulus of semiconductor nanocrystals from first-principles calculations. *Phys. Rev. B* **82**, 235321 (2010).
18. Lin, F. *et al.* Molecular and atomic adsorption of hydrogen on TiO<sub>2</sub> nanotubes: An *ab initio* study. *Chem. Phys. Lett.* **475**, 82–85 (2009).
19. Nunzi, F. & De Angelis, F. DFT investigations of formic acid adsorption on single-wall TiO<sub>2</sub> nanotubes: Effect of the surface curvature. *The J. Phys. Chem. C* **115**, 2179–2186 (2010).
20. Lisovski, O., Piskunov, S., Zhukovskii, Y. F. & Ozolins, J. *Ab initio* modeling of sulphur doped TiO<sub>2</sub> nanotubular photocatalyst for water-splitting hydrogen generation. In IOP Conference Series: Materials Science and Engineering, vol. 38, 012057 (IOP Publishing, 2012).
21. Jin, Z., Liu, C., Qi, K. & Cui, X. Photo-reduced Cu/CuO nanoclusters on TiO<sub>2</sub> nanotube arrays as highly efficient and reusable catalyst. *Sci. Reports* **7**, 39695 (2017).
22. Yadav, H. M. *et al.* Preparation and characterization of copper-doped anatase TiO<sub>2</sub> nanoparticles with visible light photocatalytic antibacterial activity. *J. Photochem. Photobiol. A: Chem.* **280**, 32–38 (2014).
23. Evarestov, R. A., Zhukovskii, Y. F., Bandura, A. V. & Piskunov, S. Symmetry and models of single-walled TiO<sub>2</sub> nanotubes with rectangular morphology. *Cent. Eur. J. Phys.* **9**, 492–501 (2011).
24. Bandura, A. & Evarestov, R. From anatase (101) surface to TiO<sub>2</sub> nanotubes: Rolling procedure and first principles LCAO calculations. *Surf. Sci.* **603**, L117–L120 (2009).
25. Momeni, M. M., Ghayeb, Y. & Ghonchehi, Z. Fabrication and characterization of copper doped TiO<sub>2</sub> nanotube arrays by *in situ* electrochemical method as efficient visible-light photocatalyst. *Ceram. Int.* **41**, 8735–8741 (2015).
26. Hohenberg, P. & Kohn, W. Inhomogeneous electron gas. *Phys. Rev.* **136**, B864 (1964).
27. Dudarev, S., Botton, G., Savrasov, S., Humphreys, C. & Sutton, A. Electron-energy-loss spectra and the structural stability of nickel oxide: An LSDA+U study. *Phys. Rev. B* **57**, 1505 (1998).
28. Hu, Z. & Metiu, H. Choice of U for DFT+U calculations for titanium oxides. *The J. Phys. Chem. C* **115**, 5841–5845 (2011).
29. Adán, C., Marugán, J., Sánchez, E., Pablos, C. & Van Grieken, R. Understanding the effect of morphology on the photocatalytic activity of TiO<sub>2</sub> nanotube array electrodes. *Electrochimica Acta* **191**, 521–529 (2016).
30. Wang, J. *et al.* Structures, electronic properties, and hydrogen-storage capacity of single-walled TiO<sub>2</sub> nanotubes. *Phys. E: Low-dimensional Syst. Nanostructures* **41**, 838–842 (2009).
31. Park, J. H., Kim, S. & Bard, A. J. Novel carbon-doped TiO<sub>2</sub> nanotube arrays with high aspect ratios for efficient solar water splitting. *Nano Lett.* **6**, 24–28 (2006).
32. Tokudome, H. & Miyauchi, M. N-doped TiO<sub>2</sub> nanotube with visible light activity. *Chem. Lett.* **33**, 1108–1109 (2004).
33. Macak, J. M. *et al.* TiO<sub>2</sub> nanotubes: Self-organized electrochemical formation, properties and applications. *Curr. Opin. Solid State Mater. Sci.* **11**, 3–18 (2007).
34. Mor, G. K., Varghese, O. K., Paulose, M., Shankar, K. & Grimes, C. A. A review on highly ordered, vertically oriented TiO<sub>2</sub> nanotube arrays: Fabrication, material properties, and solar energy applications. *Sol. Energy Mater. Sol. Cells* **90**, 2011–2075 (2006).
35. Momeni, M. M., Ghayeb, Y. & Davarzadeh, M. Single-step electrochemical anodization for synthesis of hierarchical WO<sub>3</sub>-TiO<sub>2</sub> nanotube arrays on titanium foil as a good photoanode for water splitting with visible light. *J. Electroanal. Chem.* **739**, 149–155 (2015).
36. Momeni, M. M. & Ghayeb, Y. Fabrication, characterization and photoelectrochemical behavior of Fe-TiO<sub>2</sub> nanotubes composite photoanodes for solar water splitting. *J. Electroanal. Chem.* **751**, 43–48 (2015).
37. Momeni, M. M. & Nazari, Z. Preparation of TiO<sub>2</sub> and WO<sub>3</sub>-TiO<sub>2</sub> nanotubes decorated with pbo nanoparticles by chemical bath deposition process: A stable and efficient photo catalyst. *Ceram. Int.* **42**, 8691–8697 (2016).
38. Liu, B. *et al.* Theoretical kinetic analysis of heterogeneous photocatalysis by TiO<sub>2</sub> nanotube arrays: The effects of nanotube geometry on photocatalytic activity. *The J. Phys. Chem. C* **116**, 7471–7479 (2012).
39. Zhang, Z. *et al.* Highly reduced TiO<sub>2-x</sub> nanotube arrays with enhanced visible-light absorption and room-temperature ferromagnetism. *Mater. Lett.* **69**, 89–91 (2012).
40. Ly, N. T. *et al.* Optical properties of TiO<sub>2</sub> nanotube arrays fabricated by the electrochemical anodization method. *Adv. Nat. Sci. Nanosci. Nanotechnol.* **5**, 015004 (2013).
41. Hongo, K., Watson, M. A., Iitaka, T., Aspuru-Guzik, A. & Maezono, R. Diffusion Monte Carlo study of para-diiodobenzene polymorphism revisited. *J. Chem. Theory Comput.* **11**, 907–917 (2015).
42. Scanlon, D. O. *et al.* Effect of Cr substitution on the electronic structure of CuAl<sub>1-x</sub>Cr<sub>x</sub>O<sub>2</sub>. *Phys. Rev. B* **79**, 035101 (2009).
43. Bocharov, D., Piskunov, S., Zhukovskii, Y. F., Spohr, E. & D'yachkov, P. N. First principles modeling of 3d-metal doped three-layer fluorite-structured TiO<sub>2</sub> (4, 4) nanotube to be used for photocatalytic hydrogen production. *Vac.* **146**, 562–569 (2017).
44. Simamora, A. J., Hsiung, T., Wang, H. P. & Liao, C. Photocatalytic splitting of water on Cu-TiO<sub>2</sub> nanotubes. In *Advanced Materials Research*, vol. 699, 662–666 (Trans Tech Publ, 2013).
45. Giannozzi, P. *et al.* Quantum ESPRESSO: A modular and open-source software project for quantum simulations of materials. *J. physics: Condens. matter* **21**, 395502 (2009).
46. Vanderbilt, D. Soft self-consistent pseudopotentials in a generalized eigenvalue formalism. *Phys. Rev. B* **41**, 7892 (1990).
47. Perdew, J. P., Burke, K. & Ernzerhof, M. Generalized gradient approximation made simple. *Phys. Rev. Lett.* **77**, 3865 (1996).
48. Morgan, B. J. & Watson, G. W. A DFT+U description of oxygen vacancies at the TiO<sub>2</sub> rutile (110) surface. *Surf. Sci.* **601**, 5034–5041 (2007).
49. Morgan, B. J., Scanlon, D. O. & Watson, G. W. Small polarons in Nb- and Ta-doped rutile and anatase TiO<sub>2</sub>. *J. Mater. Chem.* **19**, 5175–5178 (2009).
50. Morgan, B. J. & Watson, G. W. Intrinsic N-type defect formation in TiO<sub>2</sub>: A comparison of rutile and anatase from GGA+U calculations. *The J. Phys. Chem. C* **114**, 2321–2328 (2010).
51. Vu, N. H. *et al.* Anatase-rutile phase transformation of titanium dioxide bulk material: A DFT+U approach. *J. Physics: Condens. Matter* **24**, 405501 (2012).
52. Hart, J. N., Parker, S. C. & Lapkin, A. A. Energy minimization of single-walled titanium oxide nanotubes. *ACS nano* **3**, 3401–3412 (2009).
53. Young, M. J., Holder, A. M., George, S. M. & Musgrave, C. B. Charge storage in cation incorporated α-MnO<sub>2</sub>. *Chem. Mater.* **27**, 1172–1180 (2015).
54. Hou, L., Bu, Q., Li, S., Wang, D. & Xie, T. Ni<sub>3</sub>S<sub>2</sub>-decorated TiO<sub>2</sub> nanotube arrays as effective photoanodes for photoelectrochemical water splitting. *RSC Adv.* **6**, 99081–99087 (2016).

55. Su, W. S., Leung, T. C. & Chan, C. T. Work function of single-walled and multiwalled carbon nanotubes: First-principles study. *Phys. Rev. B* **76**, 235413 (2007).
56. Wang, Y. *et al.* Origin of magnetic properties in carbon implanted ZnO nanowires. *Sci. reports* **8**, 7758 (2018).
57. Na-Phattalung, S. *et al.* First-principles study of native defects in anatase TiO<sub>2</sub>. *Phys. Rev. B* **73**, 125205 (2006).
58. Shirley, R., Kraft, M. & Inderwildi, O. R. Electronic and optical properties of aluminium-doped anatase and rutile TiO<sub>2</sub> from *ab initio* calculations. *Phys. Rev. B* **81**, 075111 (2010).
59. Labat, F., Baranek, P. & Adamo, C. Structural and electronic properties of selected rutile and anatase TiO<sub>2</sub> surfaces: An *ab initio* investigation. *J. Chem. Theory Comput.* **4**, 341–352 (2008).
60. Muscat, J., Swamy, V. & Harrison, N. M. First-principles calculations of the phase stability of TiO<sub>2</sub>. *Phys. Rev. B* **65**, 224112 (2002).
61. Arlt, T. *et al.* High-pressure polymorphs of anatase TiO<sub>2</sub>. *Phys. Rev. B* **61**, 14414 (2000).

## Acknowledgements

Partial financial support by the research council of Shahid Bahonar University of Kerman is acknowledged. The computations in this work has been performed using the facilities of the Center for Information Science in JAIST. R.M. is grateful for financial support from MEXT-KAKENHI (17H05478 and 16KK0097), from FLAGSHIP2020 (project nos. hp170269 and hp180175 at K-computer), from Toyota Motor Corporation, and from I-O DATA Foundation.

## Author Contributions

S.K.G., M.A. and R.M. were involved in preparation of the manuscript and it was written through contributions of all authors. All authors reviewed the manuscript and approved its final version.

## Additional Information

**Competing Interests:** R.M. is funded by Toyota Motor Corporation, from I-O DATA Foundation, and from the Air Force Office of Scientific Research. S.K.G. and M.A. declare no potential conflict of interest.

**Publisher's note:** Springer Nature remains neutral with regard to jurisdictional claims in published maps and institutional affiliations.



**Open Access** This article is licensed under a Creative Commons Attribution 4.0 International License, which permits use, sharing, adaptation, distribution and reproduction in any medium or format, as long as you give appropriate credit to the original author(s) and the source, provide a link to the Creative Commons license, and indicate if changes were made. The images or other third party material in this article are included in the article's Creative Commons license, unless indicated otherwise in a credit line to the material. If material is not included in the article's Creative Commons license and your intended use is not permitted by statutory regulation or exceeds the permitted use, you will need to obtain permission directly from the copyright holder. To view a copy of this license, visit <http://creativecommons.org/licenses/by/4.0/>.

© The Author(s) 2018